



ISSN 0975-413X
CODEN (USA): PCHHAX

Der Pharma Chemica, 2016, 8(24):36-41
(<http://www.derpharmachemica.com/archive.html>)

Theoretical Studies of 4-[(6-ethoxy benzothiazol-2-yl) diazenyl] Phenyl 2-(2,3-dihydro-1H-inden-2-yl) Acetate

Mahesh Bhat*, Belagali SL

Department of Studies in Environmental Science, University of Mysore, Manasagangotri, Mysuru, Karnataka, India

ABSTRACT

The title compound $C_{26}H_{23}N_3O_3S$ was synthesized by Steglich esterification of 4-[(6-ethoxy benzothiazol-2-yl) diazenyl] phenol with Indan-2-ylacetic acid. Density functional theory at the B3LYP/TZ2P level was employed to calculate structural properties like, UV-Visible, FT-IR, HOMO-LUMO, Band gap energy and Hirshfeld surface. The Theoretical results of UV-Visible and FT-IR spectra were compared with the experimental results. Hirshfeld surface analysis was carried out for displaying the all intermolecular interactions by quantifying them in 2D finger print plot within the crystal and study confirms the important role of $\pi \rightarrow \pi$ stacking interactions.

Keywords: Crystallization, Benzothiazole, Esterification, DCC, DFT, HOMO-LUMO

INTRODUCTION

Benzothiazole is one of the most important heterocyclic compounds which have received overwhelming response owing to its diversified molecular design and remarkable biological importance [1]. Benzothiazole is a thermally stable electron-withdrawing moiety with numerous applications; it is also used as a potential component in Nonlinear Optics (NLO) for an example riluzole. In the literature many efforts have done to study of the azo bridged benzothiazole derivatives. 6-methoxy substituted alkoxy benzothiazole azo compounds show the mesogenic properties [2] and unsymmetrical azo methane substituted benzothiazoles exhibit very good opto-electrical properties [3]. Some of the 6-substituted benzothiazole azo compounds containing alkyl ester groups were synthesized and found to that, they exhibit anisotropic properties [4]. In recent years, benzothiazole moiety based LC compounds containing azomethine ($-C=N-$), azo ($-N=N-$) and ester ($-COO-$) as central linkages have been extensively studied, because benzothiazole molecule is considered as a good mesogen forming moiety [5]. The emerging applications of azo benzothiazole compounds have recently been reported in medical studies as potential sensitizers for Photodynamic Therapy (PDT), optical data storage, non-linear optics and Liquid Crystal Displays (LCDs) [6-9]. As a result, encouraged by optical and pharmacological properties of the Benzothiazole and in continuation of our interest in the synthesis of benzothiazole analogues [10-12], In order to understand molecular/electronic structure and properties of the benzothiazole ester derivatives, here we compared the results of experimental and theoretical investigations for our target ester compound.

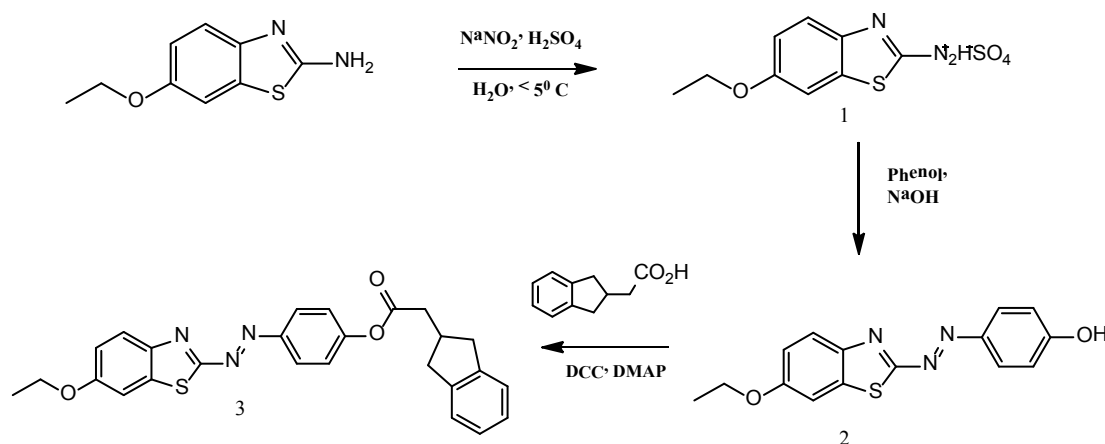
EXPERIMENTAL SECTION

MATERIALS AND METHODS

Reaction was performed in two necked 100 mL round bottom flask. The glass wares were previously rinsed with acetone and dried in hot air oven. The melting point (m.p.) was determined by open capillary method and was uncorrected. UV-Vis spectrum was recorded by UV-Visible spectrophotometer, Systronics-118. Infrared Spectra was recorded on a PerkinElmer Spectrum Version 10.03.09 and readings were taken over the range of $600-4000\text{ cm}^{-1}$. The quantum chemical calculations (DFT calculations) giving the molecular geometries of the minimum energies and molecular orbitals were performed by using the firefox -811. Energy gaps of the frontier orbitals of the crystal (HOMO-LUMO) have been determined with the B3LYP/6-31G/DP level of theory by using GAMESS software.

Synthesis and crystallization

Synthesis of (E)-4-[(6-ethoxy benzothiazol-2-yl)diazenyl] phenyl 2-(2,3-dihydro-1H-inden-2-yl)acetate: A mixture of Indan-2-ylacetic acid (0.26 g, 0.0015 mol) and DCC (0.276 g, 0.00134 mol) in MDC (10 mL) was cooled to 0°C, to that (E)-4-[(6-ethoxy benzothiazol-2-yl) diazenyl] phenol (0.4g, 0.00134 mol) and DMAP (0.164 g, 0.00134 mol) were added, the resulting suspension was stirred for 10 hrs. After completion of the reaction, it was filtered and filtrate was quenched into water (20 mL) and extracted with MDC (2 × 20 mL), dried over sodium sulphate and evaporated to dryness to get crude material, which was purified by column chromatography. The eluent was evaporated and recrystallized from ethanol, the red colored needle shape crystal was filtered and dried (0.32 g, 55%) to get title compound (Melting point: 130-131°C) (Scheme 1).



Scheme 1: Synthetic scheme

RESULT AND DISCUSSION

UV-vis spectral analysis

For the compound 3 the UV-vis spectra absorption spectra have been measured in Caron tetrachloride solution at room temperature. To compare the experimental spectra with theoretical values TD-DFT method has been applied to predict the uv-vis spectra based on the B3LYP/6-31G/DP level optimized structure.

Both the experimental and predicted UV-Vis spectrum of the compound is shown in Figure 1. From the graph, it is observed that, the compound shows absorption peak at 398.5 nm, it is due to the transition of the electron $n \rightarrow \pi^*$ transition of the ester group and absorption peaks at 426.5 nm, due to $\pi \rightarrow \pi^*$ of the N=N group. In DET studies UV-vis spectra shows the peaks at 389.27 nm and 445.96 nm and its electronic contributions are shown below.

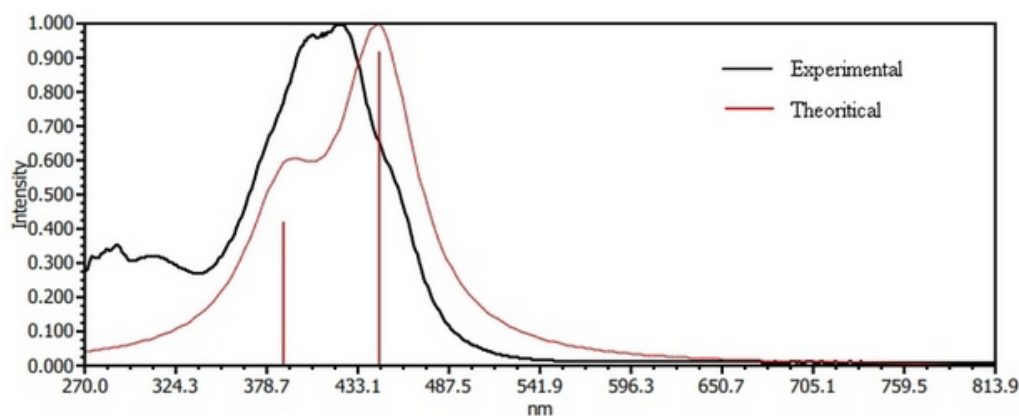


Figure 1: Experimental and theoretical vibrational spectrum (PBE/TZ2P theory level) of the crystal

Wavelength (nm):	Electronic transition mode
445.96:	HOMO->LUMO (96%)
389.27:	H-3->LUMO (90%)

FT-IR spectral analysis

The theoretical and experimental Fourier Transform Infrared Spectrum (FT IR) of the crystal is shown in the Figure 2. The experimental IR vibration frequencies are assigned as follows (DFT calculated values are within parenthesis). Comparison of the vibrations frequencies calculated at B3LYP/6-31G/DP method and experimental methods are tabulated in Table 1. DFT method

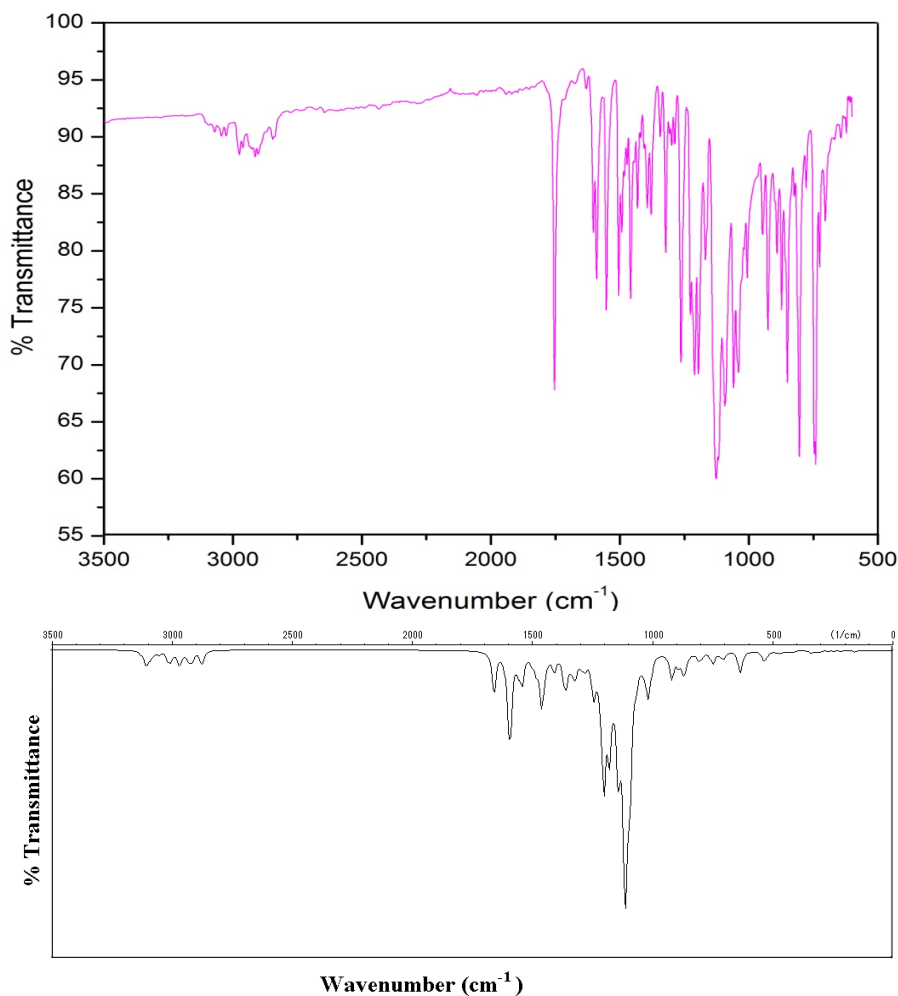


Figure 2: Experimental and theoretical FT IR spectrum of the crystal

Table 1: Compression of experimental and theoretical FT-IR peaks

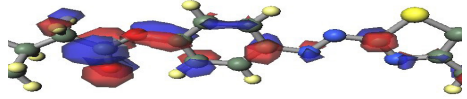
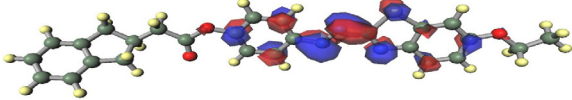
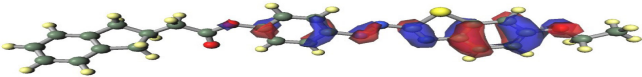
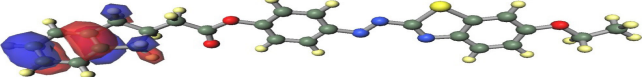
Functional groups	Experimental IR peaks in cm^{-1}	Theoretical IR frequency in cm^{-1}
C=O	1753	1727
Ar-C-H	2913	2996
C=C	1602	1657
N=N	1431	1410
C=N	1552	1520
C-N	1263	1297
C-O	1226	1228
Ali C-C	1168	1156
C-S	946	956
C-H bending	1126	1140

shows reasonably good agreement with experimental values with minor exceptions. For example C=O stretching frequency was found 1775 cm^{-1} in experimental method and 1727 cm^{-1} in theoretical method.

TD DFT calculations

In order to study the characteristics of the electronic transition and oscillator strength of the compound, a single-point, time dependent DFT calculations of lowest singlet-singlet transitions were performed by employing the B3LYP functional [13] at scalar relativistic ZORA level and the results were listed in the Table 2. In the table shows the energies of Frontier Molecular Orbitals, viz LUMO+1, LUMO, HOMO and HOMO-1 calculated using B3LYP density functional calculations. In LUMO+1 electrons are spread over the ester, phenyl and azo group, other than indane group, whereas HOMO-1 electrons are located in indane group. In general HOMO represents the bonding character and LUMO represents the antibonding character, localized over the molecule and the same concept can correlate with our molecule. The major electronic transitions of the compound exhibiting the oscillator strength and assigned to $S_0 \rightarrow S_1$, which corresponding to the HOMO- LUMO, HOMO-1-LUMO and HOMO-LUMO+1 electronic transition.

Table 2: Frontier Molecular Orbitals (FMOs) and corresponding energies

Orbital	Frontier Molecular Orbital (FMO)	Energy (in eV)
LUMO+1		-0.6259
LUMO		-2.7293
HOMO		-5.7117
HOMO-1		-6.3076

HOMO-LUMO analysis

The frontier orbitals take part in the chemical reactions, Figure 3 shows the Highest Occupied Molecular Orbitals (HOMO) and Lowest Unoccupied Molecular Orbital (LUMO) for the synthesized benzothiazole ester. It has been found that the HOMO is largely distributed over the azo group and benzothiazole ring whereas the LUMO is completely delocalized in 4-[(6-ethoxy benzothiazol-2-yl) diazenyl] phenol. From the above molecular orbital the HOMO-LUMO energy gaps have been evaluated by the DFT method.

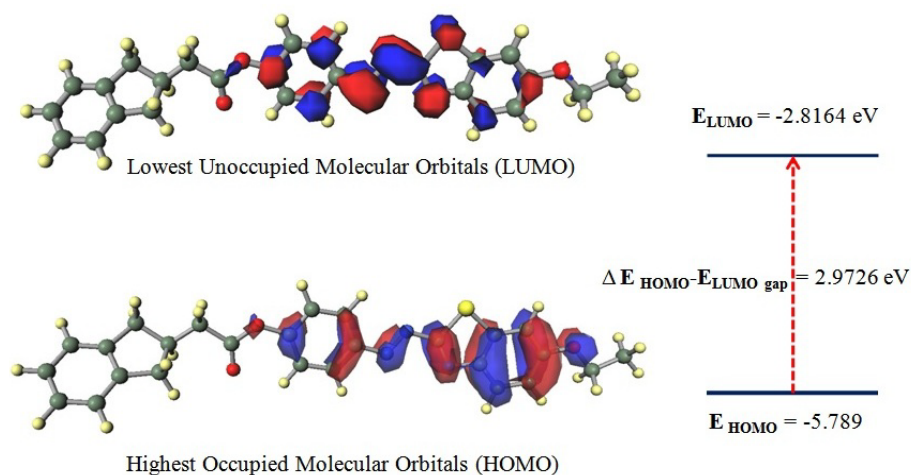


Figure 3: HOMO, LUMO and band gap energies of the crystal

From calculating the energies HOMO and LUMO, we can find out the band gap energy as follows.

$$\text{Band gap energy} = \Delta E_{\text{HOMO}} - E_{\text{LUMO}} = -5.789 - (-2.8164) = 2.9726 \text{ eV}.$$

The band gap energy calculation can correlate with the available literature and the values have shown promising in the field of organic electronics and Light Emitting Diodes (LEDs).

Arslan and Algul illustrate that, molecular structure and vibrational frequencies of the organic compound in the ground state

investigated with different functional theory method (like BLYP, B3LYP, B3PW91 etc.), comparison of the observed fundamental vibrational frequencies with experimental results indicates the B3LYP is superior [14]. In the similar way Metia *et al.* synthesized the benzothiazole derivatives and carried out the DFT studies and calculated structural and vibrational studies [15]. Hence in the present study we have compared the experimental results with results obtained from DFT method and both methods gives the almost same results.

Hirshfeld surface

The Hirshfeld surface evolved from an attempt to define the space occupied by a molecule in the crystal for the purpose of partitioning the crystal electron density into the molecular fragments [16]. In order to investigate the secondary intermolecular interactions we have analyzed the Hirshfeld surfaces of the title compound using Crystal Explorer 2.1 [17] and its surface is shown in the Figure 4a. Hirshfeld surfaces are representative of the electron distribution within the crystal and are calculated as the sum of the electronic densities of the isotropic atoms. Identification of the close contacts is made by the normalized contact distance (d_{norm}) and relative to the distance from the surface to the nearest nucleus inside and outside the surface (d_i and d_e respectively).

In the d_{norm} surface (Figure 4b) the large circular depressions are the indicators of hydrogen bonding contacts whereas other visible spots are due to H–H contacts. The dominant H–O interactions in title compound are evident in the Hirshfeld surface plots are indicated by the bright red area, also known as red hot spots (Figure 4d). The curvedness shape index surface of the compound has shown (Figure 4c and 4d), to know information about each donor and acceptor pair and shape of the surface patches. Red and blue spots in the shape index diagram (Figure 4d) are evenly distributed and it shows the $\pi \rightarrow \pi$ stacking interactions are almost identical in the crystal.

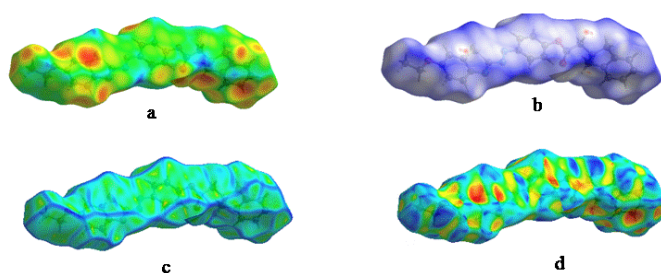


Figure 4: Hirshfeld surface a) Hf de b) $H_f d_{\text{norm}}$ c) curvedness and d) shape index of the compound

Figure 5 shows the breakdown of two dimensional finger print plots of the HS for the structure. By the analyses of the fingerprint plots d_e with d_i we can elucidate the division of contribution is possible electronic for different interactions. In the finger print plots one molecule act as a donor ($d_e > d_i$) and other as an acceptor ($d_i > d_e$). Here O–H/H–O and N–H/H–N interactions are appearing as two distinct spikes in the finger print plots and they are distributed symmetrically, for the contributions of S and O to the others $d_i > d_e$, so it can behave as acceptor atom. Blue triangles represent the convex regions due to the ring carbon atoms of the molecule inside surface. Red regions are due to the π stacked molecule above it.

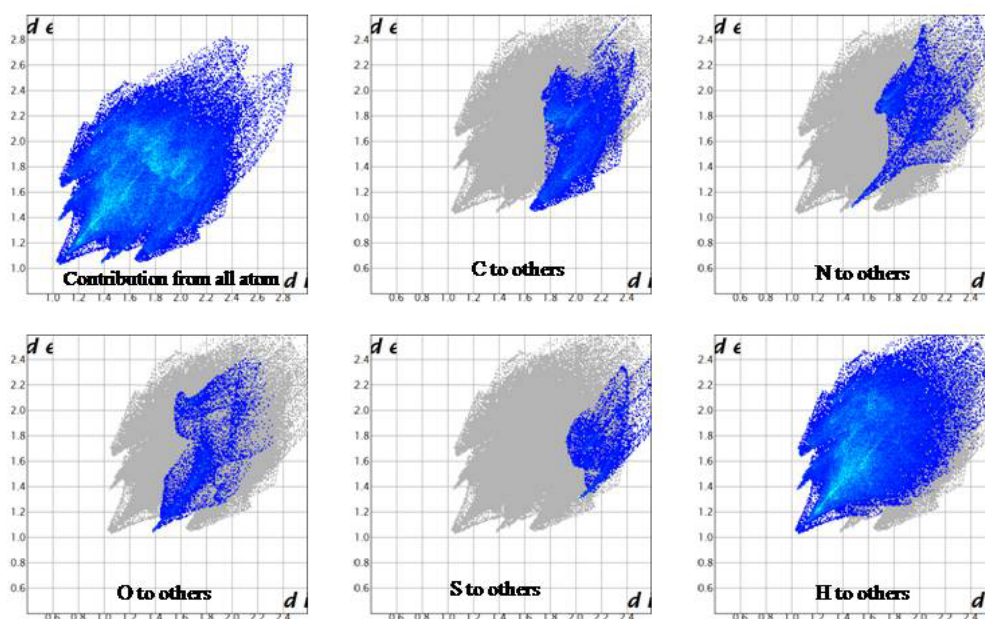


Figure 5: Fingerprint plots: Full (upper left) and different intermolecular interactions within the compound showing percentage contact contributed to the total Hirshfeld surface area of the molecule

Figure 6 shows the relative contributions of intermolecular interactions of the all the elements present in the crystal, by comparing the different elemental contribution to the HS field surface C–H/H–C contributions taking the major and it contributes 20.3 % of the total, followed by O–H/H–O (8.8 %) taking the importance. Here intermolecular interactions of O–H/H–O (8.8 %) is more compare to that of N–H/H–N (6.9 %) and S–O/ O–S (1.5 %), the enhance intermolecular interactions in O–H/H–O is due to the easy H-bond formation of the O and H atom.

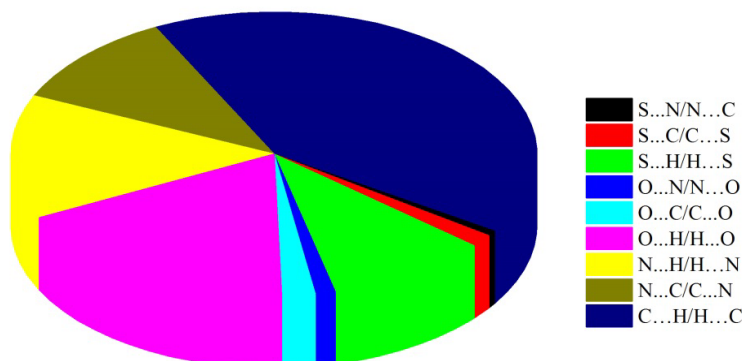


Figure 6: Relative contribution of various intermolecular interactions to the Hirshfeld surface area

CONCLUSION

Single crystal was grown by the slow evaporation method and by NMR analysis confirms the formation of title compound. The DFT based UV-Vis and FT-IR calculations were good agreement with the experimental results. Both HOMO and LUMO is delocalized over the benzothiazole and Azo phenyl group, less contribution from the oxygen atom of the ester group, whereas the HOMO-1 from indane group and LUMO+1 are contribution from ester group. Hirshfeld surface analysis was carried out for displaying the all intermolecular interactions by quantifying them in 2D finger print plot within the crystal and study confirms the important role of $\pi \rightarrow \pi$ stacking interactions.

ACKNOWLEDGEMENTS

The authors gratefully acknowledge Department of Science & Technology, Ministry of Science and Technology, New Delhi, India, for providing INSPIRE Fellowship.

REFERENCES

- [1] L.S. Khokra, K. Arora, H. Mehta, A. Aggarwal, M. Yadav, *Int. J. Pharm. Sci. Res.*, **2011**, 2(6), 1356-1377.
- [2] A.K. Prajapati, N.L. Bonde, *J. Chem. Sci.*, **2006**, 118(2), 203-210.
- [3] A. Iwan, M. Palewicz, M. Krompiec, M. Grucela-Zajac, E. Schab-Balcerzak, A. Sikora, *Spectrochimica Acta Part A: Molecular and Biomolecular Spectroscopy*, **2012**, 97, 546-555.
- [4] Y. Guan-Yeow, A. Alshargabi, M.M. Ito, W.A. Kamil Mahmood, D. Takeuchi, *Mol. Cryst. Liq. Cryst*, **2012**, 557, 126-133.
- [5] M.D.R. Karim, R. Yahya, M.D.R. Karim Sheikh, N.M. Salleh, A. Hassan, H.N.M. Ekramul Mahmud, *J. Polym. Res.*, **2014**, 21, 487.
- [6] M.M.M. Raposo, A.M.C. Fonseca, M.C.R. Castro, M. Belsley, M.F.S. Cardoso, L.M. Carvalho, P.J. Coelho, *Dyes and Pigments*, **2011**, 91(1), 62-73.
- [7] H. Faustino, R.M. El-Shishtawy, L.V. Reis, P.F. Santos, P. Almeida, *Tetrahedron Letters*, **2008**, 49(48), 6907-6909
- [8] H. Faustino, C.R. Brannigan, L.V. Reis, P.F. Santos, P. Almeida, *Dyes and Pigments*, **2009**, 83(1), 88-94.
- [9] S. Manickasundaram, P. Kannan, Q.M.A. Hassan, P.K. Palanisamy, *J. Mat. Sci. Mat. in Electron.*, **2008**, 19(11), 1045-1053.
- [10] M. Bhat, S.L. Belagali, *Res. Chem. Intermed.*, **2016**, 42(7), 6195-6208
- [11] M. Bhat, S.L. Belagali, S. Madan Kumar, K. Byrappa, *Chemical Data Collections*, **2016**, 7-8, 1-7
- [12] M. Bhat, B.S.L. Elagali, P.S. Rajesh, V. Ravishankar Rai, *Monatsh Chem.*, **2016**, 147(11), 2001-2008
- [13] <http://www.classic.chem.msu.su/gran/firefly/index.html>
- [14] H. Arslan, O. Algül, *Int. J. Mol. Sci.*, **2007**, 8, 760-776
- [15] M. Aydin, F. Jean-Mary, N. Stevens, L. Daniel Akins, *J. Phys. Chem. B.*, **2004**, 108, 9695-9702
- [16] M.A. Spackman, P.G. Byrom, *Chem. Phys. Lett.*, **1997**, 267, 215-222
- [17] S.K. Wolff, D.J. Grimwood, J.J. McKinnon, D. Jayatilaka, M.A. Spackman, "Crystal Explorer 3.0," University of Western Australia, Perth, **2007**.